Title

Structure of human rhinovirus complexed with Fab fragments from a neutralizing antibody.

Journal

Journal of virology, 67(3)

ISSN

0022-538X

Authors

Smith, TJ
Olson, NH
Cheng, RH
et al.

Publication Date

1993-03-01

DOI

10.1128/jvi.67.3.1148-1158.1993

Peer reviewed

JOURNAL OF VIROLOGY, Mar. 1993, p. 1148–1158
0022-538X/93/031148-11$02.00/0

Vol. 67, No. 3

Structure of Human Rhinovirus Complexed with Fab Fragments from a Neutralizing Antibody

THOMAS J. SMITH,[1]* NORMAN H. OLSON,[1] R. HOLLAND CHENG,[1] HANSONG LIU,[1] ELAINE S. CHASE,[1] WAI MING LEE,[2] DONNA M. LEIPPE,[2] ANNE G. MOSSER,[2] ROLAND R. RUECKERT,[2] AND TIMOTHY S. BAKER[1]

Department of Biological Sciences, Purdue University, West Lafayette, Indiana 47907,[1] and Institute for Molecular Virology, University of Wisconsin, Madison, Wisconsin 53706[2]

Received 18 September 1992/Accepted 19 November 1992

We have determined the structure of a human rhinovirus (HRV)-Fab complex by using cryoelectron microscopy and image reconstruction techniques. This is the first view of an intact human virus complexed with a monoclonal Fab (Fab17-IA) for which both atomic structures are known. The surface area on HRV type 14 (HRV14) in contact with Fab17-IA was ~500 Å^2 (5 nm^2), which is much larger than the area that constitutes the NIm-IA epitope (on viral protein VP1) defined by natural escape mutants. From modeling studies and electrostatic potential calculations, charged residues outside the neutralizing immunogenic site IA (NIm-IA) were also predicted to be involved in antibody recognition. These predictions were confirmed by site-specific mutations and analysis of the Fab17-IA-HRV14 complex, along with knowledge of the crystallographic structures of HRV14 and Fab17-IA. The bound Fab17-IA reaches across a surface depression (the canyon) and meets a related Fab at the nearest icosahedral twofold axis. By adjusting the elbow angles of the bound Fab fragments from 162° to 198°, an intact antibody molecule can be easily modeled. This, along with aggregation and binding stoichiometry results, supports the earlier proposal that this antibody binds bivalently to the surface of HRV14 across icosahedral twofold axes. One prediction of this model, that the intact canyon-spanning immunoglobulin G molecule would block attachment of the virus to HeLa cells, was confirmed experimentally.

Human rhinovirus (HRV) is a major cause of the common cold and a member of the picornavirus family, which also includes poliovirus, coxsackievirus, and hepatitis A virus. These are small, spherical viruses that have a 300-Å (1 Å = 0.1 nm)-diameter protein shell which encapsulates one copy of single-stranded RNA (32). The existence of more than 100 different serotypes of HRV makes the development of effective vaccines against the common cold impractical.

The structure of HRV serotype 14 (HRV14) is known to atomic resolution (30). The capsid is composed of 60 copies each of the four viral proteins VP1, VP2, VP3, and VP4 (Fig. 1). The first three proteins (each ~30 kDa) all have an eight-stranded, anti-parallel β-barrel motif (30, 31). The small VP4 (~10 kDa) lies at the interface between the RNA interior and the capsid. Neutralizing immunogenic sites (NIm sites) were identified on the basis of sequence analysis of natural escape mutants (33, 34). These mutants were selected for by growing the virus in the presence of monoclonal antibodies (MAbs), and the mutations were mapped onto the three-dimensional structure of the virus where they cluster into four surface groups: NIm-IA, NIm-IB, NIm-II, and NIm-III. All NIm sites occur at the rim of an ~12-Å deep canyon that encircles each of the icosahedral fivefold axes. The hypothesis that the canyon is the site at which the cell-surface receptor proteins bind (30) was recently confirmed (26, 27). Such an arrangement allows naturally occurring mutants to circumvent immune recognition without affecting receptor recognition.

The mechanisms of neutralization are poorly understood. Some antibodies are believed to bind bivalently to the same particle (15) and neutralize infectivity by inducing structural changes in the capsid (13, 21), by interfering with attachment (10), or possibly by preventing uncoating by intracapsid cross-linking (24). For HRV14 (10), the pI of the capsid is greatly reduced by the addition of intact mouse MAbs or antigen-binding fragments (Fabs). Therefore, if the pI shift is caused by antibody-induced conformational changes in the virus, such alterations are not dependent on bivalent attachment to the same virion. For some antibodies, interparticle cross-linking (aggregation) may be sufficient for neutralization (4–6, 15, 36). Past studies on picornaviruses have distinguished two classes of neutralizing antibodies, strong and weak. Strongly neutralizing antibodies are believed to bridge pentamers within the HRV14 particle (20, 24). This model predicts that each Fab arm binds to its epitope in an orientation that points the other arm toward a binding site across an icosahedral twofold symmetry axis on the same particle.

To test this latter model, we determined the structure of HRV14 complexed with Fab17-IA by using three-dimensional reconstruction of electron microscope images. MAb17-IA is a strongly neutralizing MAb (20). This immunoglobulin G (IgG) molecule binds to the NIm-IA site defined by natural escape mutations (34) at residues D1091 and E1095 (the character specifies the amino acid residue, the first digit refers to viral protein VP1, and the last three digits designate the residue number). The image reconstruction of this complex (computed to ~28-Å resolution) accurately identifies the footprint of the Fab on the virion. This is the first time that such a complex has been visualized in which the atomic structures of the Fab and virion are both known. The Fabs bind in an orientation that appears to favor interaction between Fab fragments related by the icosahedral twofold axes. The atomic structure of Fab17-IA (20a)

* Corresponding author.

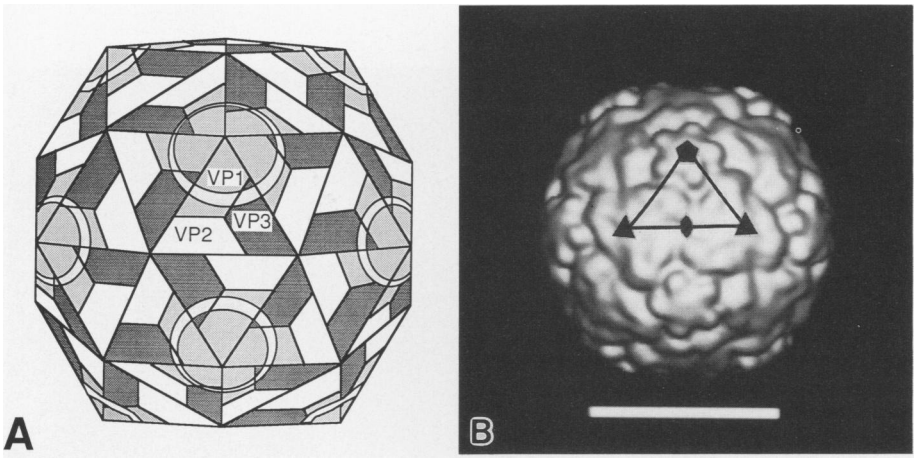

FIG. 1. Structure of HRV14. (A) Diagrammatic representation of HRV14 (30). Promoters of capsid proteins VP1, VP2, and VP3 are indicated. The canyon, or surface depression, is shown as an annulus that encircles each icosahedral fivefold axis. (B) Solid-model representation of native HRV14 computed to 20-Å resolution from the known atomic structure. One asymmetric unit, bounded by two icosahedral threefold axes and one fivefold axis, is outlined, and icosahedral five-, three-, and twofold axes are identified by a triangle, an oval, and a pentagon, respectively. The canyon appears as a depression that encircles a mass of density centered on the vertex. Bar = 200 Å.

was fit into the reconstructed electron density, and a bivalently attached antibody has been modeled. These results lend further support to the existence of antibodies bound bivalently to the same viral particle.

MATERIALS AND METHODS

MAb production. MAb17-IA was produced in mice and then later by using the Cellmax Quad 4 cell culture system (Cellco Corp., Germantown, Md.). High-glucose Dulbecco's modified Eagle medium (catalog no. 430-2100; GIBCO/Bethesda Research Laboratories, Grand Island, N.Y.) containing 10% fetal bovine serum was used for the hybridoma cell culture. The antibody is of the isotype IgG2a as determined by Screentype (Boehringer Mannheim Biochemicals, Indianapolis, Ind.). The antibody was purified by means of protein G affinity chromatography. The samples were loaded onto the affinity column, and the unbound material was washed from the column with 0.1 M, pH 7.0, sodium phosphate buffer. The antibody was then eluted with a 50 mM, pH 2.0, sodium acetate buffer and quickly neutralized with 1 M, pH 8.0, sodium phosphate buffer. MAb17-IA was pooled and dialyzed against 0.1 M, pH 7.0, sodium phosphate buffer and concentrated to 1 to 2 mg/ml.

Fab17-IA generation and purification. Papain cleavage was performed on the antibody solution at an enzyme-to-antibody ratio of 1:100 (mg/mg) at 37°C for 10 h in the presence of 25 mM β-mercaptoethanol. The reaction was stopped by the addition of 75 mM iodoacetamide. The digested sample was then dialyzed extensively against 10 mM, pH 7.5, Tris-HCl buffer and purified on a Mono-Q ion-exchange column connected to an FPLC system (Mono-Q and FPLC are trademarks of the Pharmacia/LKB Corp., Piscataway, N.J.). The proteins were eluted with an NaCl gradient of ~0.01 M/ml of eluate. The flow rate was 1 ml/min, and the pressure was 1 MPa. The pI of Fab17-IA is more than 8.0 and therefore elutes in the void volume of the column. The Fc fragments and intact MAb17-IA have much lower pIs and elute at NaCl concentrations greater than 0.1 M. Fab17-IA was pooled and concentrated with Centricon 10 microconcentrators (Amicon Corporation, Beverly, Mass.).

Fab17-IA complex preparation. Fab was added to HRV14 (prepared as previously described [14]) in a ratio of ~300 to 600 Fabs per virion at a virus concentration of ~0.25 mg/ml. The mixture was incubated overnight at 5°C and then loaded onto a Superose 6 (Pharmacia/LKB) column equilibrated with 10 mM Tris, pH 7.5, buffer with 50 mM sodium chloride. The virus-Fab complex eluted in the void volume, far removed from the unbound Fab molecules, and was then concentrated to ~10 mg/ml with Centricon 10 microconcentrators (Amicon Corp.).

Cryoelectron microscopy and image analysis. Cryoelectron microscopy of the HRV14-Fab complex was performed essentially as previously described (2, 9, 25). The sample was transferred to fresh, non-glow-discharged holey-carbon films on 400-mesh copper grids. The grids were briefly blotted with filter paper, quickly frozen in liquified ethane, transferred to liquid nitrogen, and then placed in a cooled Gatan 626 cryotransfer holder (Gatan Inc., Warrendale, Pa.) before being inserted into a Philips EM420 electron microscope (Philips Electronics Instruments, Mahwah, N.J.). Images were photographed under minimal dose conditions (<20 electrons per Å^2) at a nominal magnification of 49,000 and at ~1-μm underfocus.

Micrograph selection and digitization and selection of individual virion images was performed as previously described (9). The intensity values of the individual particle images were adjusted to remove linear background gradients (3) and to normalize the means and variances (7). Translation and orientation parameters were determined for each virion image and a data set of 35 images was selected from which a three-dimensional reconstruction was calculated to an effective resolution of 28 Å (2, 41). An eigenvalue spectrum was calculated to test for the possible presence of errors in the reconstruction because of the inclusion of nonrandom data (11). All values exceeded 10.0, indicating the uniqueness of the data included in the analysis.

The three-dimensional reconstruction was corrected for the effects of the contrast transfer function of the electron microscope (8, 37) after it was radially scaled to match the dimensions of the atomic map of HRV14 (30). The electron density map was Fourier transformed to compute structure

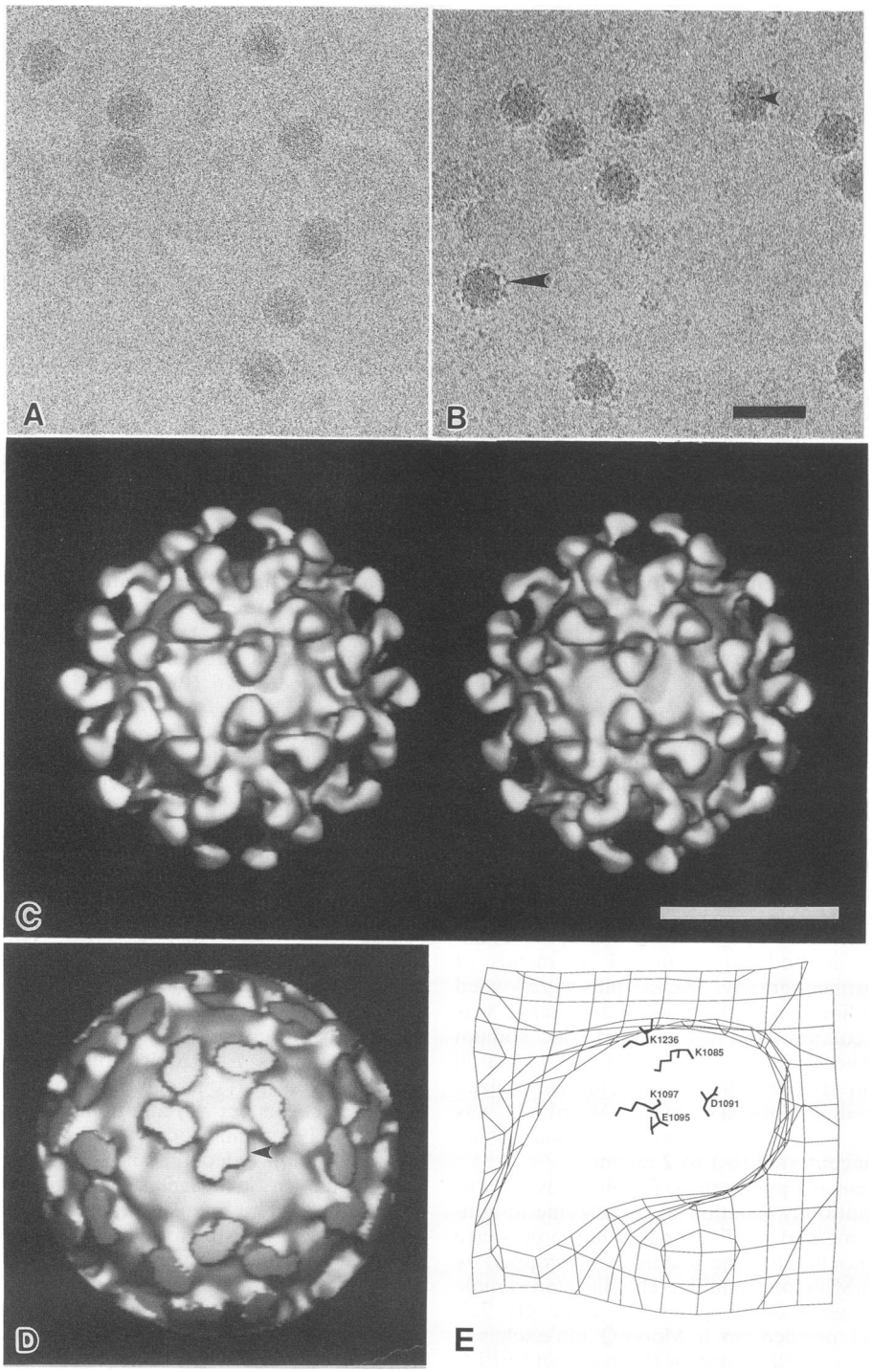

FIG. 2. Cryoelectron microscopy and image analysis of native HRV14 and HRV14-Fab17-IA complexes. (A) Native HRV14 virions exhibit relatively smooth, circular profiles. (B) HRV14-Fab17-IA complexes. Fabs are visible on the periphery of the particles (large arrowhead) and sometimes as black dots when seen end-on (small arrowhead). (C) Stereo view of a solid-model representation of the HRV14-Fab17-IA complex. (D) Solid-model representation of the contact area between Fab17-IA and HRV14. The density of the complex reconstruction was truncated at a radius of ~155 Å to show the point of contact. One footprint is indicated (arrowhead). (E) Wire model representation of the same footprint as indicated in panel D. The residues of HRV14 that were altered in escape mutants (Table 1) are labeled. Bar = 500 Å (panels A and B); 200 Å (panel C).

TABLE 1. Effect of mutations in HRV14 on binding affinity of MAb17-IA

Virus	Binding affinity (10^9 M^{-1})[a]
Wild type	180
K1085E[b]	46
D1091N[c]	<0.2
E1095K[c]	<0.2
K1097E[b]	5
K1236E[b]	74

[a] K_d was measured by the ability of antibody to precipitate 50% of the ^{35}S-labeled virions.

[b] Constructed by site-directed mutagenesis (19). Mutants K1085E and K1236E were unable to make plaques under conditions originally employed for selecting spontaneous escape mutants. Mutant K1097E made tiny plaques even in the absence of antibody; its poorer growth and inconspicuous plaques could explain why it was not picked up in the original screen for spontaneous escape mutants.

[c] Spontaneous escape mutants (34) were selected for the ability to make plaques in the presence of excess antibody.

factors which were then multiplied by an empirical inverse contrast transfer function that was derived from a model based on the X-ray structure of HRV14 (8). A corrected map was produced by Fourier synthesis of the modified structure factors and displayed on an ESV30 vector graphics device (Evans and Sutherland Computer Corporation, Salt Lake City, Utah).

Site-specific mutagenesis of HRV14. Mutagenesis (19) was performed with uracil-enriched single-stranded DNA of a subclone containing VP1 plus flanking segments of VP3 and protein 2A (bases 2113 to 3206). The mutagenic primers were synthesized in the Biotechnology Center, University of Wisconsin. The primers were then purified with a SepPak C_{18} cartridge (Waters Chromatography Division, Millipore Corporation, Milford, Mass.). Phosphorylation of primers, synthesis of the mutated strands with T4 DNA polymerase, ligation, and transformation were performed as previously described (18). Approximately 80% of the transformants contained mutant plasmids. The cassette regions of selected mutant plasmids were completely sequenced to confirm the in vitro DNA synthesis fidelity. The mutations were transplanted into the full-length clone as *Crf*10I-*Dra*III or *Dra*III-*Ppu*MI fragments. Each full-length clone was linearized by *Mlu*I restriction enzyme digestion. The runoff RNA transcripts, synthesized in vitro by T7 RNA polymerase, were transfected into 188-mm^2 monolayers of H1-HeLa cells (2.5 million cells) with DEAE-dextran. Viruses were recovered after a 2-day incubation at 35°C. The virus stock was amplified and labeled with [^{35}S]methionine as previously described (19). Labeled virus particles were purified on sucrose density gradients.

Binding stoichiometry determination. ^{3}H-HRV14 (5×10^{10} virions; 6×10^7 PFU) of known specific activity (1.7×10^5 cpm/μg) was incubated with ^{35}S-labeled MAb at various antibody-to-virus ratios in 100 μl of phosphate-buffered saline containing 1% bovine serum albumin (PBSA). After an overnight incubation at room temperature, the immune complexes in a single sample were sedimented on 5 ml of 5 to 20% (wt/wt in PBSA) sucrose gradients for 22 min at 225,000 × *g* to separate antibody-monomeric virion immune complexes from the aggregated immune complexes. The stoichiometry of antibody binding was determined by using the monomeric immune complexes.

Effects of MAb17-IA on HRV14 cell attachment. The effect of MAb17-IA on cell receptor binding was determined with intact HeLa cells. PBSA (25 μl) containing various concentrations of MAb17-IA was added to 5.6×10^{11} ^{35}S-virions in 3.5 ml of PBSA. The mixtures were incubated at 8°C overnight, and 1.5 ml of each mixture was added to cell pellets containing 6×10^7 HeLa cells (4,000 virions per cell) which had been washed twice with PBSA in a 15-ml capped, conical tube. As a control for virus-MAb17-IA precipitation, 1.5 ml of each mixture was placed in a tube that did not contain cells. The cell pellets were resuspended and then incubated for 1 h at 23°C. The samples were centrifuged for 5 min at 23°C at 450 × *g*, the supernatants were removed, and the radioactivity was measured. The cell pellets were resuspended in 1.5 ml of PBSA, and the radioactivity was measured. All scintillation data were used to calculate the percentage of virus bound to the cells.

Immune precipitation measurements. Purified ^{35}S-labeled HRV14 was incubated with purified antibody at various antibody-to-virus ratios for 1 h at room temperature and subsequently overnight at 4°C. Each sample (5×10^7 PFU per ml; 6×10^{10} virions per ml) contained about 3×10^4 cpm in a final volume of 100 ml of PBSA. The percentage of virus in the pellet after a 5-min microcentrifugation at 16,000 × *g* was determined by measuring the radioactivity in the supernatants and in the pellets. Calculations indicated that aggregates of approximately 35 or more virions would pellet in this assay.

RESULTS AND DISCUSSION

Analysis of the reconstructed density map. Native HRV14 particles appeared very smooth and featureless in cryoelectron micrographs (Fig. 2A). In comparison, images of vitrified HRV14-Fab complexes appeared fuzzy because of the bound Fab molecules. Some Fabs could be seen edge-on at the periphery of the particles and occasionally end-on nearer the centers of the particle images (Fig. 2B).

A shaded, surface representation of the native HRV14 X-ray structure (30) was computed to 20 Å (Fig. 1B) for comparison with the structure of HRV14 in the reconstructed HRV14-Fab17-IA complex (Fig. 2C). The most prominent features of the native HRV14 surface include (i) a pentameric dome of density at each icosahedral vertex, (ii) a depression or canyon which surrounds each vertex, and (iii) triangular plateaus of density centered at each of the 20 icosahedral threefold axes. In the areas where the bound Fab17-IA does not occlude the view, each of these features is seen on the surface representation of the three-dimensional reconstruction of the complex (Fig. 2C). The triangular plateaus have similar enantiomorphic features in both the X-ray and image reconstruction maps, which enables the hand of the reconstruction to be established unambiguously. Since the capsids in both maps contain such similar features, it appears that the Fab17-IA binding does not induce any large conformational changes in the virion. A comparison of the structure of native HRV14 and the reconstruction was further examined by means of the three-dimensional graphics program FRODO (16) which also did not reveal any large conformational changes. Sixty Fabs are bound to the virion surface, with five surrounding each of the 12 vertices. The electron density of the Fab fragments was approximately at the same level as that of the viral protein shell, implying full saturation of the 60 available antigenic sites. Each Fab is an elongated, bilobed structure which extends ~75 Å above the virus surface and has a maximum cross-section of ~40 Å.

The site to which Fab17-IA binds was previously identi-

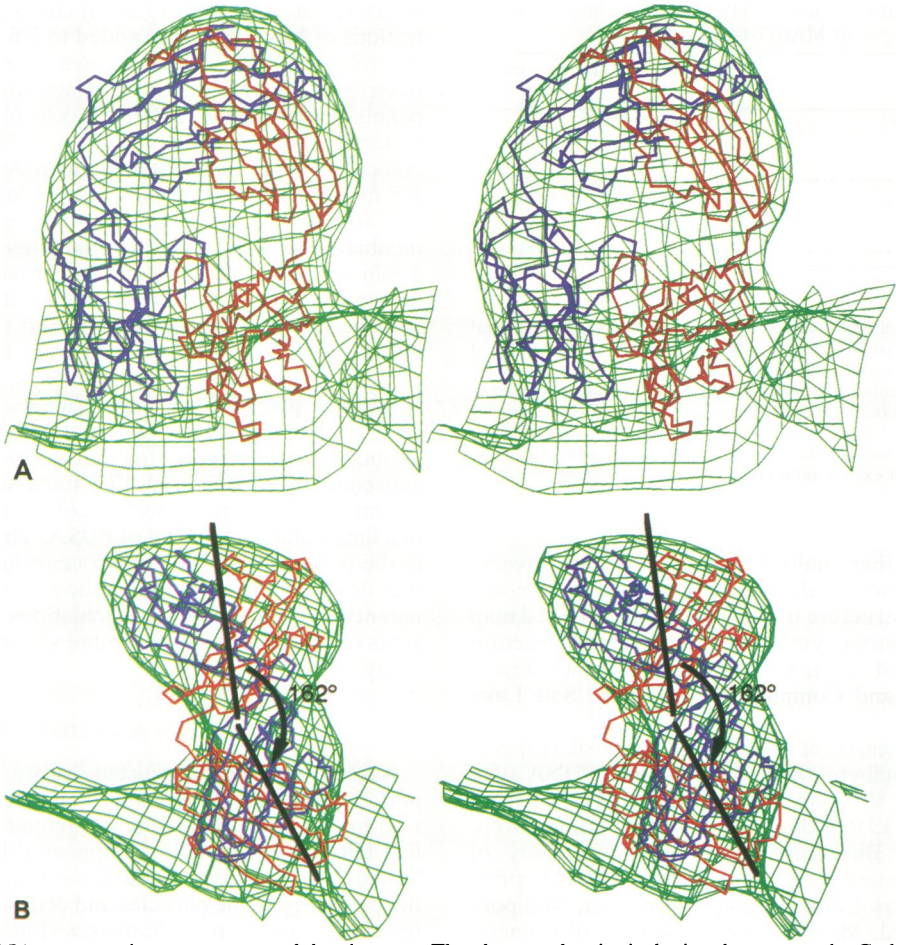

FIG. 3. Fit of Fab17-IA structure into reconstructed density map. The electron density is depicted as green; the Cα backbone of the heavy chain is red; and the Cα backbone of the light chain is dark blue. (A) The view direction is approximately from a fivefold axis of the virus toward an icosahedral twofold axis. The variable domain of the Fab is toward the bottom. (B) Same as panel A except view direction is rotated 90° about the vertical direction.

fied with spontaneous escape mutations to neutralizing antibodies (33, 34) and with site-specific mutations (19). Natural escape mutant sites D1091 and E1095 are on an external loop of VP1 between the B and C strands of the β-barrel of VP1. Using computer simulations (see below) based on the crystallographically determined structure of the antibody, it was possible to match the electrostatic charge pattern on the binding surface of the Fab molecule with a complementary charge pattern found on the crystallographically determined surface of HRV14. This docking model not only included the charge residues D1091 and E1095, previously identified by escape mutation analysis, but also predicted the involvement of three additional charged residues, K1085, K1097, and K1236.

It was also possible to define an antibody footprint (Fig. 2D) by computationally trimming away from the image shown in Figure 2C all of the electron density at a radius exceeding 155 Å. This footprint included all five of the charge-matched residues (Fig. 2E) identified in the docking model described above.

These residues were changed by means of site-specific mutagenesis, and the mutants exhibited reduced binding affinity for MAb17-IA (Table 1). The mutation sites most effective at abrogating antibody binding (D1091, E1095, and K1097) were located near the center of the footprint (Fig. 2E). The least effective mutation sites (K1085 and K1236) were at the edge. Therefore, the mutational analysis agrees very well with the reconstructed density of the HRV14-Fab complex.

Fit of the crystallographic structure of Fab17-IA into the reconstructed Fab density. The atomic structure of Fab17-IA has been recently determined (20a). The R-factor of the current model for all reflections between 6- and 2.7-Å resolution is approximately 20% (solvent molecules not yet included). The elbow angle of the crystallized Fab is about 162°. The elbow angle is defined as the angle between the pseudo-dyad axes in the variable and constant domains that relate the heavy and light chains. An elbow angle of less than 180° places the variable and constant β-barrels of the heavy chain in contact with each other.

The Fab17-IA structure matches the reconstructed density determined by electron microscopy remarkably well (Fig. 3). The reconstructed Fab density contains two globular regions that are separated by a constriction or dimple. These regions and the dimple correspond to the constant, variable, and elbow regions, respectively. If the elbow angle of the Fab17-IA structure were ~180°, then the positioning of the Fab into the reconstructed density would be ambiguous

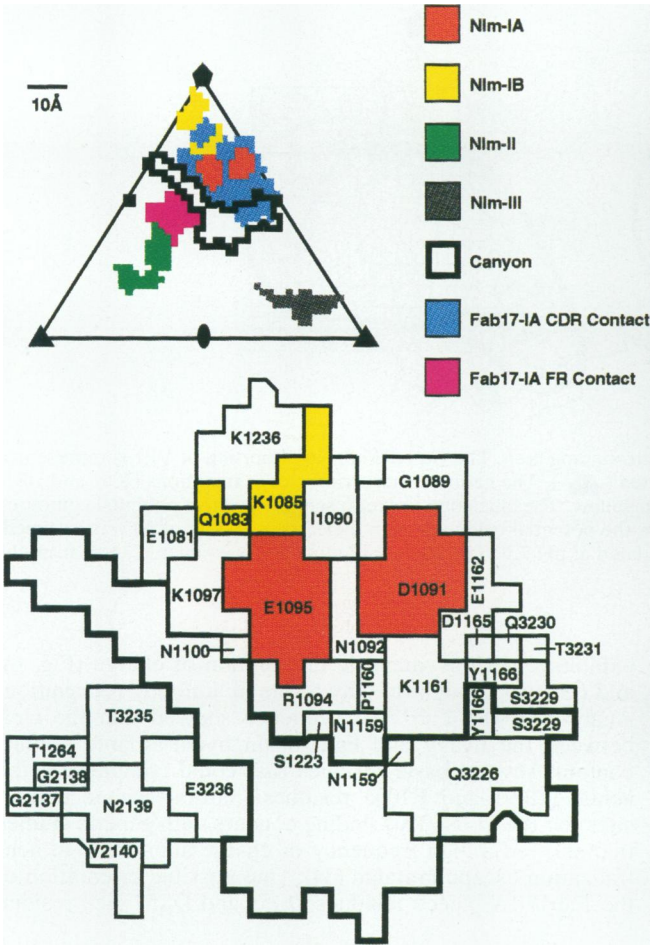

FIG. 4. Representation of surface residues within an asymmetric unit of HRV14. The canyon, which encircles each of the fivefold axes, is outlined by a thick black line. The NIm sites and residues in contact with the Fab CDR and FR regions are represented by different colors. The icosahedral fivefold (north pole) and twofold (south pole) axes are labelled by a pentagon and an ellipse, respectively. Identity of the residues shown in the triangular asymmetric unit are shown in the detail below.

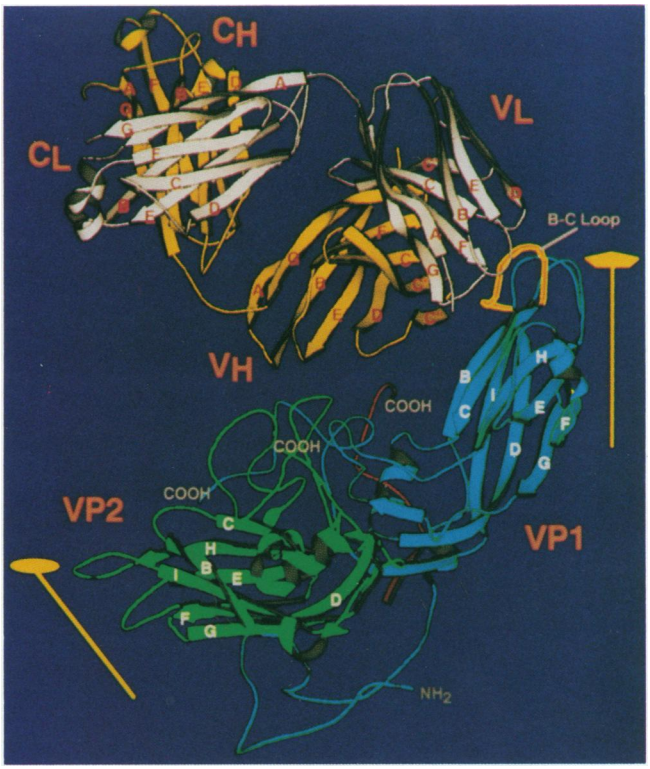

FIG. 5. Ribbon drawing (17) of Fab17-IA model docked to HRV14. VP1 is blue, VP2 is green, and a small piece of VP3 is shown in red. The light and heavy chains of the Fab are white and yellow, respectively. The B-C loop of VP1 (the NIm-IA site) is highlighted in orange. V_H, V_L, C_H, and C_L represent the variable heavy chain, variable light chain, constant heavy chain, and constant light chain β-barrels, respectively. The twofold (⬬) and fivefold (⬟) icosahedral axes are indicated.

since the structures of the heavy and light chains are so similar. Because the elbow angle of Fab17-IA is 162°, only one orientation of the structure correlates well with the electron density.

Although the resolution of the reconstruction in this study is ~28 Å, the positioning of the Fab and its interactions with HRV14 can be described to a much higher resolution. This phenomenon is similar to what is seen in most protein X-ray crystallographic studies. A resolution of ~1 to 1.5 Å is necessary to observe the individual atoms of a molecule, but most protein crystals diffract X rays only to a resolution of 2 to 3 Å. It is only by knowledge of the amino acid sequence and the expected stereochemistry of the molecules that crystallographers are able to describe protein structures in atomic detail at 2- to 3-Å resolution. In an analogous way, the current study describes details to a resolution greater than 28 Å because the atomic structures of Fab17-IA and HRV14 are both known. As was observed in a previously reported Fab-virus complex (38), the positioning of the Fab structure into the electron density appears to be accurate to ~4 Å. In addition, recent electron microscopy studies of other icosahedral viruses have accurately described details at a much higher resolution than that of the reconstructions. Small protrusions were observed at the threefold axes of the bacteriophage ϕX174 image reconstruction (23). The crystallographic structure of ϕX174 showed that each of the protrusions accurately corresponded to a bundle of three α-helices that consisted of only 33 amino acid residues (25). Even more striking was a recent electron microscopy study of flock house virus (9a) in which density was observed at the internal RNA-protein interface. This density was ascribed to tightly bound, genomic RNA that was also observed in the crystallographic structure (14a).

Each Fab17-IA appeared to cover at least 500 Å^2 or ~one-quarter of the asymmetric unit surface. This contact area overlaps the receptor-binding region of the canyon (26, 27) and the NIm-IB site and also touches the NIm-II site (Fig. 4). The area of contact shown in Fig. 4 represents a conservative lower-limit estimate and is very likely to increase when crystallographic evidence of the virus-Fab complex becomes available. The Fab forms a bridge over the canyon, connecting the north and south walls (Fig. 5). This may explain previous experiments demonstrating that MAb-34, another IgG directed against the NIm-IA site, blocks HRV14 binding to purified cell membranes (10).

The more conserved framework portion of the variable region (FR) near the elbow may contact the south wall of the

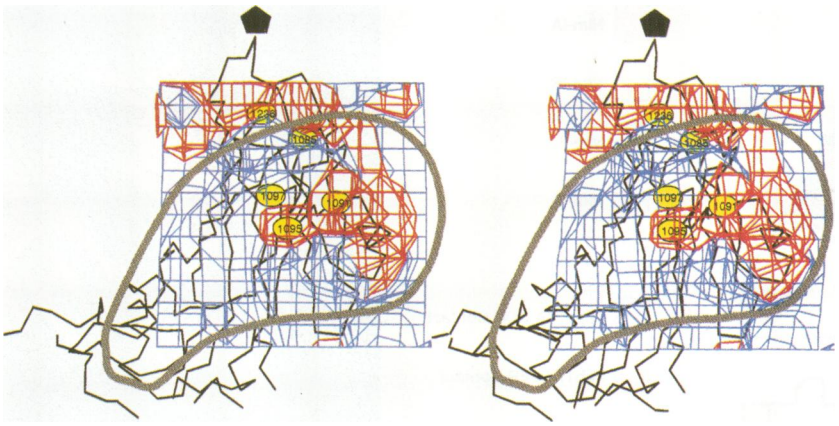

FIG. 6. Electrostatic potential map of NIm-IA site of HRV14 and surrounding area. The Cα backbone of a portion of VP1 is represented by black lines, and the position of the icosahedral fivefold axis is indicated (⬟). The naturally occurring escape mutations (1091 and 1095) as well as the site-specific mutations (1085, 1097, and 1236) are labelled in yellow. The blue contours represent the positive potential contoured at 30 mV, and the red represents the negative potential at −30 mV. For the potential calculations, a dielectric constant of 50 was assumed, and the effective pK values for Arg, Lys, His, Glu, and Asp were calculated at pH 7.0. The potential function was evaluated away from the charge centers by using a finite difference method (39, 40).

canyon near the NIm-II site (Fig. 4 and 5). The significance of this observation needs to be studied further with bound IgG molecules since such interactions might disappear when MAb17-IA binds bivalently.

Electrostatic interactions between Fab17-IA and HRV14. Theoretical studies have suggested that electrostatic potential is an important determinant of protein-protein interactions (39). Prior to the present studies, we performed docking experiments, using charge and shape complementarity as guides for modeling antibody binding. The NIm-IA region exhibits a very asymmetric distribution of charge (Fig. 6), and this was thought to play a role in antibody recognition. Analysis of the Fab17-IA sequence showed that the cleft between the heavy and light chain hypervariable regions contains several basic residues that could complement the acidic D1091 and E1095 residues (natural escape mutant sites) on the virus. This finding concurs with genetic studies that showed a high frequency of charge alterations in neutralization escape mutants (34). One possible orientation of the Fab17-IA placed residues D_H55 and D_H57 (see residue

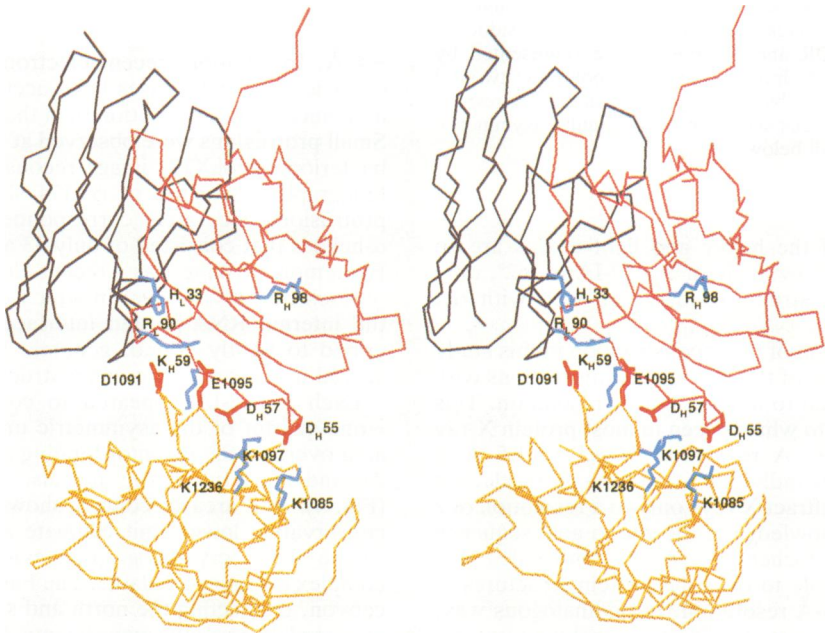

FIG. 7. Electrostatic interactions between docked Fab17-IA and HRV14. For Fab17-IA residues, the amino acids are numbered sequentially, and the chain type is designated by a subscript following the one-letter amino acid code. The Cα backbone of the V_L domain of Fab17-IA is dark blue, and the Cα of V_H domain is deep red. A portion of the Cα backbone of HRV14 VP1 is shown in orange. The acidic side chains around the epitope are shown in red, and the basic side chains are shown in blue. For clarity, all of the charged residues in the Fab17-IA hypervariable region are shown, whereas only the escape mutation sites are shown on the HRV14 surface.

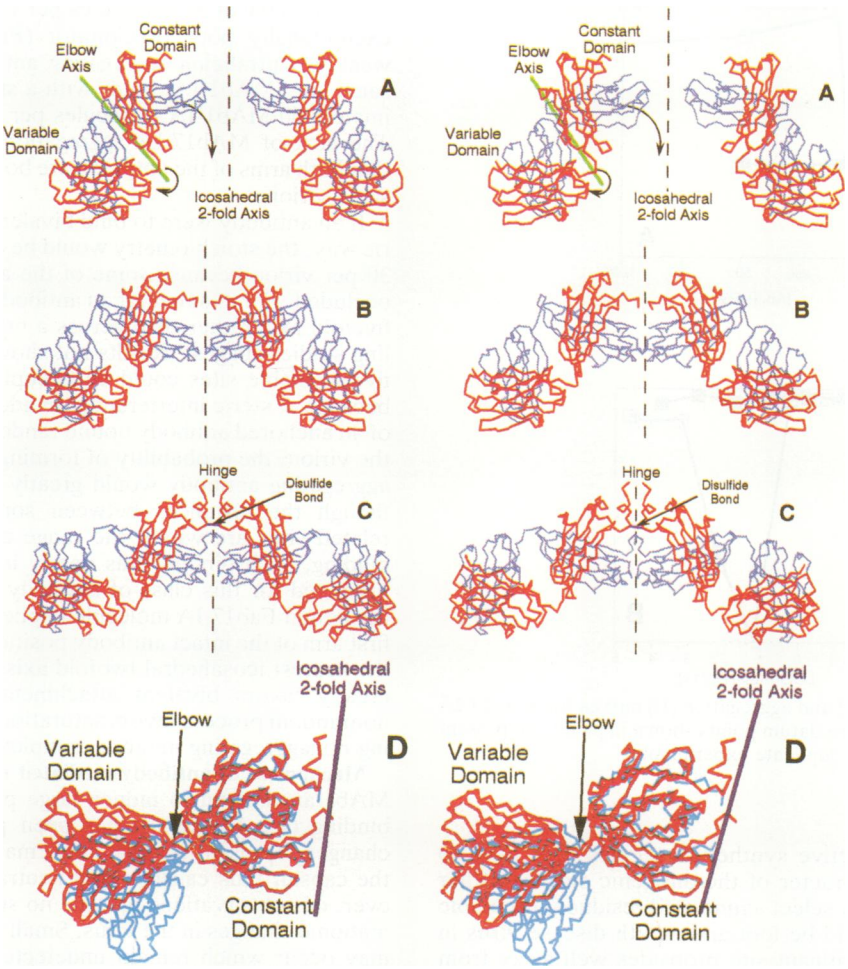

FIG. 8. (A) Cα backbone of icosahedral twofold-related Fab17-IA molecules as observed in the image reconstruction. The icosahedral twofold axis is represented by a dashed line, and the elbow axis is represented by a thick green line. The arrows indicate how the constant domain was rotated about the elbow angle to produce the $(Fab17\text{-}IA)_2$ structure shown in panel B. The surface of the virion is at the bottom of the diagram. The heavy chain is depicted in red, and the light chain is depicted in blue. (B) An $(Fab17\text{-}IA)_2$ model produced by rotating the constant domains of the bound, twofold-related Fab17-IA molecules. The variable domain remained fixed to the surface of the virion during these rotations. (C) Cα backbone of Kol for comparison to the modeled $(Fab17\text{-}IA)_2$ molecule. The twofold axis of Kol coincides with the icosahedral twofold axis shown in Fig. 6A and B. (D) The Cα backbones of the altered Fab17-IA structure from Fig. 6B overlaid onto the Cα backbone of Kol as oriented in Fig. 6C. The elbow axis, Kol, and Fab17-IA are shown in green, red, and blue, respectively.

designation in Fig. 7) of the loop between βD and βE of the heavy chain complementarity-determining region 2 (CDR2) near a cluster of three lysine residues on the surface of HRV14 (K1097, K1085, and K1236).

Fab17-IA and HRV14 probably form complementary electrostatic surfaces upon binding (Fig. 7). Residues K_H59 and R_L90 might be able to form salt bridges with residues E1095 and D1091, respectively, when Fab17-IA is bound to the surface of HRV14. While not in direct contact with E1095 or D1091, H_L33 and R_H98 might enhance the binding of the NIm-IA loop by increasing the overall basic character of the cleft. In addition to the interactions with the acidic NIm-IA loop, D_H55 and D_H57 of the bound Fab17-IA are appropriately positioned to bind to K1097 of HRV14. K1085 and K1236 are also in proximity to D_H55 and D_H57, with K1236 being the farthest away. These interactions correspond very well with the site-specific mutation studies. For the three mutated lysines, the abrogation of antibody binding was proportional to proximity of the mutation site to D_H55 and D_H57 of the bound Fab17-IA (Table 1), with changes at residues K1085 and K1236 causing only marginal effects.

The structural fit between the bound Fab17-IA and HRV14 is very good, although some of the interactions are closer than expected for van der Waals contacts (Fig. 7). This may reflect small inaccuracies in fitting the Fab17-IA structure into the density, or it may indicate that small conformational changes occur in the two proteins during the immune reaction. Indeed, minor structural rearrangements have been observed in high-resolution antigen-antibody crystallographic studies (29).

From our results, we would predict that a peptide representing the NIm-IA loop would be a poor antigen. Residue K1097 is clearly essential for antibody binding. Although K1097 is close in sequence to the natural escape mutation sites D1091 and E1095, the side chain is much closer to the surface of the virion. In addition, mutational analysis of residues 1236 and 1085 demonstrated that they do play a role in antibody binding despite being quite distal to the NIm-IA

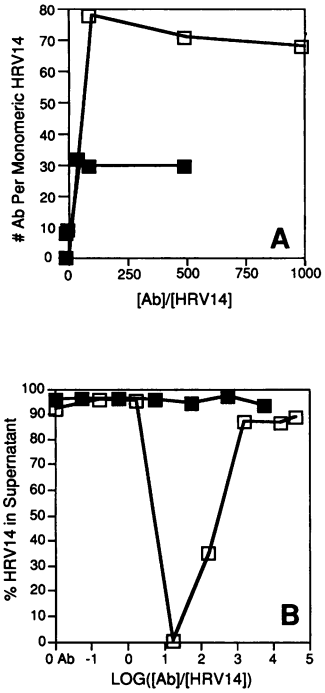

FIG. 9. Saturation (A) and aggregation (B) curves for MAb17-IA (■) and MAb1-IA (□). The datum points shown in panel A represent the average values from duplicate experiments.

loop. Therefore, effective synthetic vaccines may have to mimic the charge character of the antigenic surface rather than just contain a few select amino acid residues. A notable exception to this would be foot-and-mouth disease virus in which the immunodominant site protrudes well away from the surface of the virion (1).

Bivalent attachment model. The orientation of the bound Fab fragments, pointing toward each other across the twofold symmetry axis, was consistent with earlier proposals that the intact IgG molecule binds bivalently to the surface of HRV14. Consequently, we modeled the conformation of intact antibodies bound to HRV14, using the observed orientation of the bound Fab17-IA in the reconstruction. The constant domains of icosahedrally twofold-related, bound Fab17-IA molecules (Fig. 8A) were rotated about the elbow axes by approximately 36° toward the surface of the virion (Fig. 8B) to a final elbow angle of 198°. Such rotation places the two Fab17-IA constant domains in the same relative orientations as observed in the intact antibody Kol (22) (Fig. 8C). When the twofold axis of Kol coincides with this icosahedral twofold axis, the positions and orientations of the constant domains in Fab17-IA and Kol match exceedingly well (Fig. 8D). Therefore, it is possible to model a bivalently bound antibody with minimal conformational rearrangement of the bound Fab structure.

The proposed bivalently attached antibody requires an elbow angle greater than 180°. While all published Fab structures have an elbow angle less than 180°, an Fab structure has been recently determined (to 2.2 Å) that has an elbow angle of 192° (20b). Therefore, the elbow angles in the proposed bivalently bound MAb17-IA molecule are unusual but not impossible.

Binding and aggregation studies strongly support the proposed bivalent attachment model. MAb17-IA binds with a stoichiometry of 30 antibodies per virion (Fig. 9A) and is an exceptionally poor precipitator (Fig. 9B). In contrast, a weakly neutralizing aggregating antibody that binds to the same site (MAb1-IA) binds with a stoichiometry of approximately 60 MAb1-IA molecules per virion (Fig. 9A and B). The lack of MAb17-IA aggregation supports the proposal that both arms of the antibody are bound to the surface of the same virion.

If an antibody were to bind bivalently, but in an asymmetric way, the stoichiometry would be expected to be less than 30 per virion because some of the available sites would be occluded. For example, if an antibody were to bind around a fivefold axis rather than across a twofold axis, then modelling studies suggest (results not shown) that only two of the five available sites could be occupied by bound Fab arms because of steric interference. In addition, if the second arm of an anchored antibody bound randomly to available sites of the virion, the probability of forming a monovalently bound aggregating antibody would greatly increase. Finally, even though the distances between some other icosahedrally related sites are within the range consistent with bivalent binding, such binding was nearly impossible to model. As predicted for this class of antibody (24), the orientation of the bound Fab17-IA molecule implies that the binding of the first arm of the intact antibody positions the other arm across the nearest icosahedral twofold axis in an orientation which greatly favors bivalent attachment. This highly ordered nonrandom process favors saturation of available sites yielding nonaggregating immune complexes.

Mechanism of antibody-mediated neutralization. Fabs and MAbs are known to induce large pI shifts in virions upon binding (10, 13, 21). It has been proposed that these pI changes represent a large conformational rearrangement of the capsid, thus causing viral neutralization (13, 21). However, our observations provide no support for gross conformational changes in the virus. Small conformational changes may occur which remain undetected at ~30 Å resolution. Indeed, as has been observed with high-resolution antigen-Fab complexes (29), some antibody and antigen structural rearrangements are very likely to occur during the immune reaction. However, such small conformational changes are unlikely to decrease the pI of the virions from 7 to 3 as observed with HRV14 neutralization (10). Therefore, the change in pI may be due to changes in exposed surfaces due to MAb or Fab binding rather than structural rearrangement of the virion.

Perhaps one of the most important effects of antibody

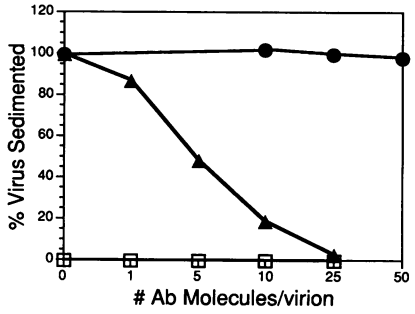

FIG. 10. Effect of MAb17-IA on attachment of native HRV14 (▲) and the genetically engineered K1097E escape mutant (●) to HeLa cell suspensions. As a control, the percentage of virus-MAb17-IA complex sedimenting in the absence of cells is also shown (□).

binding in vitro is to block viral interactions with the cellular receptor. As shown in Fig. 10, five to six MAb17-IA molecules are sufficient to block attachment of HRV14 by 50%. Under these conditions, a control lacking HeLa cells showed no detectable precipitation (cell-associated virus) of virus-antibody complexes at any of the antibody concentrations tested. Since previous studies demonstrated that Fabs can also block attachment of the virion to cell membrane preparations (10), bivalent binding of the MAb to the same virion is not required to block attachment. The difference in neutralization efficacies between the various antibodies may be due to the difference between the binding affinities of monovalently and bivalently attached antibodies. It is also possible that, as is the case with antiviral compounds to rhinovirus (12, 28), antibodies have more than one neutralizing mechanism. Both monovalently and bivalently bound antibodies might interfere with cell receptor interactions, but bivalently bound antibodies may be more effective because they can also stabilize the capsid by cross-linking the icosahedral pentameric units (24).

ACKNOWLEDGMENTS

This work was supported by National Institute of Health grants GM10704 to T.J.S., AI24939 and AI31960 to R.R.R., and GM33050 to T.S.B., by National Science Foundation grant DMB-8905062 to T.S.B., and by the Lucille P. Markey Charitable Trust (Purdue Structural Biology Center).

We thank M. G. Rossmann for stimulating discussions and advice, C. Music for photography, and J. C. Bell for preparation of the manuscript. The programs FRODO (16) and MacInPlot (35) were used to create Fig. 2 through 8.

ADDENDUM IN PROOF

We have just completed the image reconstruction of the MAb17-IA-HRV14 complex. As predicted in this article, this complex clearly shows MAb17-IA bivalently bound across icosahedral twofold axes, no significant conformational changes in the capsid structure, the constant region of the Fab fragments still in contact with the south wall of the canyon, and rotation of the constant domains about the elbow axes upon bivalent attachment. However, this rotation is probably not 36° as predicted by the Kol model but rather ~15 to 18°. The hinge region of the bound MAb17-IA appears to be more like that observed in the very recent determination of the structure of an intact mouse antibody of the same isotype as MAb17-IA (L. J. Harris, S. B. Larson, K. W. Hasel, J. Day, A. Greenwood, and A. McPherson, Nature [London] **360**:369–372, 1992).

REFERENCES

1. **Acharya, R., E. Fry, D. Stuart, G. Fox, D. Rowlands, and F. Brown.** 1989. The three-dimensional structure of foot-and-mouth disease virus at 2.9Å resolution. Nature (London) **327**: 709–716.
2. **Baker, T. S., W. W. Newcomb, N. H. Olson, L. M. Cowsert, C. Olson, and J. C. Brown.** 1991. Structures of bovine and human papilloma viruses: analysis by cryoelectron microscopy and three-dimensional image reconstruction. Biophys. J. **60**:1445–1456.
3. **Booy, F. P., W. W. Newcomb, B. L. Trus, J. C. Brown, T. S. Baker, and A. C. Steven.** 1991. Liquid-crystalline, phage-like packing of encapsidated DNA in herpes simplex virus. Cell **64**:1007–1015.
4. **Brioen, P., D. Dekegel, and A. Boeyé.** 1983. Neutralization of poliovirus by antibody-mediated polymerization. Virology **127**: 463–468.
5. **Brioen, P., B. Rombaut, and A. Boeyé.** 1985. Hit-and-run neutralization of poliovirus. J. Gen. Virol. **66**:2495–2499.
6. **Brioen, P., A. A. M. Thomas, and A. Boeyé.** 1985. Lack of quantitative correlation between the neutralization of poliovirus and the antibody-mediated pI shift of the virions. J. Gen. Virol. **66**:609–613.
7. **Carrascosa, J. L., and A. C. Steven.** 1978. A procedure for evaluation of significant structural differences between related arrays of protein molecules. Micron **9**:199–206.
8. **Cheng, R. H.** 1992. Correlation of cryo-electron microscopic and X-ray data and compensation of the contrast transfer function. Proc. Electron Microsc. Soc. Am. **50**:996–997.
9. **Cheng, R. H., N. H. Olson, and T. S. Baker.** 1992. Cauliflower mosaic virus: a 420 subunit (T=7), multilayer structure. Virology **186**:655–668.

9a. **Cheng, R. H., N. H. Olson, J. E. Johnson, and T. S. Baker.** Unpublished results.

10. **Colonno, R. J., P. L. Callahan, D. M. Leippe, and R. R. Rueckert.** 1989. Inhibition of rhinovirus attachment by neutralizing monoclonal antibodies and their Fab fragments. J. Virol. **63**:36–42.
11. **Crowther, R. A.** 1971. Procedures for three-dimensional reconstruction of spherical viruses by Fourier synthesis from electron micrographs. Philos. Trans. R. Soc. Lond. B **261**:221–230.
12. **Diana, G. D., M. A. McKinlay, M. J. Otto, V. Akullian, and C. Oglesby.** 1985. [[(4,5-Dihydro-2-oxazolyl)phenoxy]alkyl]isoxazoles. Inhibitors of picornavirus uncoating. J. Med. Chem. **28**:1906–1910.
13. **Emini, E. A., P. Ostapchuk, and E. Wimmer.** 1983. Bivalent attachment of antibody onto poliovirus leads to conformational alteration and neutralization. J. Virol. **48**:547–550.
14. **Erickson, J. W., E. A. Frankenberger, M. G. Rossmann, G. S. Fout, K. C. Medappa, and R. R. Rueckert.** 1983. Crystallization of a common cold virus, human rhinovirus 14: "isomorphism" with poliovirus crystals. Proc. Natl. Acad. Sci. USA **80**:931–934.

14a. **Fisher, A. J., and J. E. Johnson.** Ordered duplex RNA controls the capsid architecture of an icosahedral animal virus. Nature (London), in press.

15. **Icenogle, J., H. Shiwen, G. Duke, S. Gilbert, R. Rueckert, and J. Anderegg.** 1983. Neutralization of poliovirus by a monoclonal antibody: kinetics and stoichiometry. Virology **127**:412–425.
16. **Jones, T. A.** 1982. A graphics model building and refinement system for macromolecules, p. 303–317. *In* D. Sayre (ed.) Computational crystallography. Clarendon Press, Oxford.
17. **Kraulis, P. J.** 1991. MOLSCRIPT: a program to produce both detailed and schematic plots of protein structures. J. Appl. Crystallog. **24**:946–950.
18. **Kunkel, T. A., J. D. Roberts, and R. A. Zakour.** 1987. Rapid and efficient site-specific mutagenesis without phenotypic selection. Methods Enzymol. **154**:367–382.
19. **Lee, W. M.** 1992. Ph.D. thesis. University of Wisconsin, Madison.
20. **Leippe, D. M.** 1991. Ph.D. thesis. University of Wisconsin, Madison.

20a. **Liu, H., and T. J. Smith.** Unpublished data.

20b. **Love, R.** Personal communication.

21. **Mandel, B.** 1976. Neutralization of poliovirus: a hypothesis to explain the mechanism and the one-hit character of the neutralization reaction. Virology **69**:500–510.
22. **Marquart, M., J. Deisenhofer, R. Huber, and W. Palm.** 1980. Crystallographic refinement and atomic models of the intact immunoglobulin molecule Kol and its antigen-binding fragment at 3.0Å and 1.9Å resolution. J. Mol. Biol. **141**:369–391.
23. **McKenna, R., D. Xia, P. Willingman, L. L. Ilag, S. Krishnaswamy, M. G. Rossmann, N. H. Olson, T. S. Baker, and N. L. Incardona.** 1992. Atomic structure of single-stranded DNA bacteriophage ϕX174 and its functional implications. Nature (London) **355**:137–143.
24. **Mosser, A. G., D. M. Leippe, and R. R. Rueckert.** 1989. Neutralization of picornaviruses: support for the pentamer bridging hypothesis, p. 155–167. *In* B. Semler and E. Ehrenfeld (ed.), Molecular aspects of picornavirus infection and detection. American Society for Microbiology, Washington, D.C.
25. **Olson, N. H., T. S. Baker, P. Willingmann, and N. L. Incardona.**

1992. The three-dimensional structure of frozen-hydrated bacteriophage ϕX174. J. Struct. Biol. **108:**168–175.

26. **Olson, N. H., P. R. Kolatkar, M. A. Oliveira, R. H. Cheng, J. M. Greve, A. McClelland, T. S. Baker, and M. G. Rossmann.** Structure of a human rhinovirus complexed with its receptor molecule. Proc. Natl. Acad. Sci. USA, in press.
27. **Olson, N. H., T. J. Smith, P. R. Kolatkar, M. A. Oliveira, R. R. Rueckert, J. M. Greve, M. G. Rossmann, and T. S. Baker.** 1992. Cryoelectron microscopy of complexes of human rhinovirus with a monoclonal FAB and the viral cellular receptor. Proc. Electron Microsc. Soc. Am. **50:**524–525.
28. **Pevear, D. C., F. J. Fancher, P. J. Felock, M. G. Rossmann, M. S. Miller, G. Diana, A. M. Treasurywala, M. A. McKinlay, and F. Dutko.** 1989. Conformational change in the floor of the human rhinovirus canyon blocks adsorption to HeLa cell receptors. J. Virol. **63:**2002–2007.
29. **Rini, J. M., U. Schulze-Gahmen, and I. A. Wilson.** 1992. Structural evidence for induced fit as a mechanism for antibody-antigen recognition. Science **255:**959–965.
30. **Rossmann, M. G., E. Arnold, J. W. Erickson, E. A. Frankenberger, J. P. Griffith, H. J. Hecht, J. E. Johnson, G. Kamer, M. Luo, A. G. Mosser, R. R. Rueckert, B. Sherry, and G. Vriend.** 1985. Structure of a human common cold virus and functional relationship to other picornaviruses. Nature (London) **317:**145–153.
31. **Rossmann, M. G., and J. E. Johnson.** 1989. Icosahedral RNA virus structure. Annu. Rev. Biochem. **58:**533–573.
32. **Rueckert, R. R.** 1990. Picornaviridae, p. 507–548. *In* B. N. Fields and D. M. Knipe (ed.), Virology. Raven Press, New York.
33. **Sherry, B., A. G. Mosser, R. J. Colonno, and R. R. Rueckert.** 1986. Use of monoclonal antibodies to identify four neutralization immunogens on a common cold picornavirus, human rhinovirus 14. J. Virol. **57:**246–257.
34. **Sherry, B., and R. R. Rueckert.** 1985. Evidence for at least two dominant neutralization antigens on human rhinovirus 14. J. Virol. **53:**137–143.
35. **Smith, T. J.** 1990. MacInPlot—a program to display electron density and atomic models on the MacIntosh personal computer. J. Appl. Crystallog. **23:**141–142.
36. **Thomas, A. A. M., P. Brioen, and A. Boeyé.** 1985. A monoclonal antibody that neutralizes poliovirus by cross-linking virions. J. Virol. **54:**7–13.
37. **Toyoshima, C., and N. Unwin.** 1988. Contrast transfer for frozen-hydrated specimens: determination from pairs of defocused images. Ultramicroscopy **25:**279–292.
38. **Wang, G., C. Porta, Z. Chen, T. S. Baker, and J. E. Johnson.** 1992. Identification of a Fab interaction footprint site on an icosahedral virus by cryoelectron microscopy and X-ray crystallography. Nature (London) **355:**275–278.
39. **Warwicker, J.** 1989. Investigating protein-protein interaction surfaces using a reduced stereochemical and electrostatic model. J. Mol. Biol. **206:**381–395.
40. **Warwicker, J., and H. C. Watson.** 1982. Calculations of the electric potential in the active site cleft due to α-helix dipoles. J. Mol. Biol. **157:**671–679.
41. **Winkelmann, D. A., T. S. Baker, and I. Rayment.** 1991. Three-dimensional structure of myosin subfragment-1 from electron microscopy of sectioned crystals. J. Cell Biol. **114:**701–713.